





Ecological Impact Patterns and Temporal Cycles of Green Tide Biomass in the Settlement Region: Based on Time-Series Remote Sensing and In Situ Data

Guangzong Zhang , Lifeng Niu , Mengquan Wu , *Member, IEEE*, Hermann Kaufmann, Hanyu Li , Yufang He , and Bo Chen , *Member, IEEE*

Abstract—Recurring green tides (also called *Ulva prolifera*) cause significant damage to marine ecosystems in the Yellow Sea of China, especially in the settlement region. The settlement region is a critical area for the natural decay and decomposition of green tides, which obviously has ecological consequences. Recent studies in relation to this topic are mostly based on point observation data, which prevents to quantitatively analyze the ecological impact patterns of green tide biomass at large spatial scales. Therefore, we used remote sensing time-series of Geostationary Ocean Color Imager satellite data combined with in situ data to invert marine chlorophyll-a (Chl-a, main indicators representing phytoplankton biomass) concentrations by machine learning methods. Finally, based on a cross-satellite model, we quantified the green tide biomass that occurred in Haiyang City during 2015 and 2016. The main results found are as follows. First, the green tide biomass reveals negative correlations on Chl-a concentration in the settlement region. The Chl-a concentration showed a decreasing trend and remained at a low level ($0.1\text{--}0.2\text{ mg/m}^3$) when the biomass of the green tide increased. After the disappearance of the green tides, the Chl-a concentration accreted rapidly and then began to gradually decrease. Second, combined with the pixel-based statistics grid of the green tide and the average Chl-a concentration, the time cycle of green tides in the settlement region is about 30–35 d. Finally, some special cases (such as typhoon) can change the pattern and temporal cycle in the settlement region. This article provides support for marine ecosystem monitoring.

Index Terms—Biomass, chlorophyll-a (Chl-a), green tide, machine learning.

Manuscript received 5 May 2023; revised 14 July 2023 and 12 September 2023; accepted 24 November 2023. Date of publication 4 December 2023; date of current version 19 December 2023. This work was supported in part by the National Key Research and Development Program of China under Grant 2022YFD2401202, in part by the Natural Science Foundation of Guangdong Province under Grant 2022A1515010113, and in part by the Natural Science Foundation of Shenzhen City under Grant GXWD20220811163556003. (*Lifeng Niu is co-first author.*) (*Corresponding author: Bo Chen.*)

Guangzong Zhang, Lifeng Niu, Hanyu Li, Yufang He, and Bo Chen are with the Institute of Space Science and Applied Technology, Harbin Institute of Technology, Shenzhen 518055, China (e-mail: 20b958035@stu.hit.edu.cn; 20b958034@stu.hit.edu.cn; lihanyu608608@163.com; 19b958025@stu.hit.edu.cn; hitchenbo@hit.edu.cn).

Mengquan Wu is with the College of Resources and Environmental Engineering, Ludong University, Yantai 264025, China (e-mail: ld_wmq@ldu.edu.cn).

Hermann Kaufmann is with the Institute of Space Science, Shandong University at Weihai, Weihai 264209, China (e-mail: hkauf@sdu.edu.cn).

Digital Object Identifier 10.1109/JSTARS.2023.3338979

I. INTRODUCTION

WITH the uncontrolled development and utilization of marine resources, ecological damage has become a serious phenomenon, resulting in frequent occurrence of marine ecological calamities. In recent years, algae disasters caused by marine eutrophication have been widely reported in China's coastal waters, and have gradually developed into one of the major disasters affecting marine ecology [1], [2]. Green tides are a kind of macroalgal blooms (MABs), which are typically formed by *Ulva Prolifera* (*U. prolifera*), belonging to the genus of *Ulva*. Green tides were first discovered in 2007 and recurred till today in the Yellow Sea, China [3], [4], [5], [6]. Research indicates that *U. prolifera* grows and expands extensively under suitable conditions due to its flexible reproduction strategies and plastic morphological adaptations [7], [8]. Approximately, 3.0×10^5 tons of MABs accumulate on the sea surface each year, most of which decompose in the natural environment, whereas only 4%–6% of the algae are salvaged and disposed [9], [10]. Floating green tides outbreak absorb a large amount of nutrients and release allelochemical secretions, thereby inhibiting the growth of phytoplankton and seriously disrupting the ecosystem balance in the sea areas [11], [12], [13], [14], [15].

In recent years, various remote sensing technologies and methods have been used to monitor macroalgal disasters. The normalized difference vegetation index, the enhanced vegetation index, and other methods are applied to data recorded by optical satellite sensors like Moderate Resolution Images Spectroradiometer (MODIS), Korean Geostationary Ocean Color Imager (GOCI), Landsat-5/TM (Thematic Mapper), Landsat-8/OLI (Operational Land Imager), Sentinel-2 MSI (Multispectral Instrument), HJ-1/CCD, Gaofen-1, and others [14], [15], [16], [17], [18]. In this context, Hu et al. [19] proposed a floating algae index (FAI) and applied it to MODIS satellite data. This method exhibits superior accuracy compared to other algorithms and demonstrates reduced sensitivity to environmental changes, even under conditions of thin cloud cover. The high-precision and robust algae computing index provides the possibility to monitor the distribution and biomass of green tides on a large scale.

As an important primary producer within the marine ecosystem, phytoplankton is an essential source of energy. It converts solar energy into chemical energy for storage, fixation, and

transfer to the next trophic level through the photosynthetic pigment chlorophyll-a (Chl-a) [20], [21], [22]. The Chl-a content is related to the biomass of phytoplankton. With the development of machine learning and deep learning, many different models were used to invert the Chl-a [23], [24], [25], [26], [27]. Unlike laboratory research, the inversion of Chl-a concentrations by the use of remotely sensed data is not limited by time-consuming field works and restricted traditional on-site sample collections. It can better resolve spatial distribution and timely changes during the actual growth period. After comparing several machine learning methods (such as multilayer perceptron, artificial neural network, and support vector machine), Hu et al. [28] inverted the global ocean surface Chl-a through a support vector regression (SVR) method and showed that this machine learning method has the best performance. All these studies show the feasibility of using machine learning methods for the inversion of Chl-a concentrations from remotely sensed images.

Recurring green tide disasters cause significant damage to marine ecosystems in the Yellow Sea, especially near settlement regions. Floating algae sink to the sea floor and subsequently decompose. During this process, massive biogenic elements are released, mainly in the form of reduced nitrogen and phosphate into seawater, interfering with the circulation and distribution of nutrients in the Yellow Sea [29], [30]. At the same time, the death of large-scale green tide in this region has a significant effect on the phytoplankton community [31], [32]. Many studies show that the settlement region of floating green tides has obviously ecological consequences [11], [33]. Recent research identified the southeastern part of Shandong Peninsula as the main settlement region of *U. prolifera* in the Yellow Sea [34]. And as such, it is necessary to clarify the ecological impact pattern of green tides in the settlement regions. However, current studies are mostly focusing on point-based sampling techniques [35], [36], [37], [38], and thus, there is a lack of synoptic spatial observations and a quantitative exploration of the green tide biomass on the marine ecological environment.

Due to the aforementioned reasons, we analyzed green tides, based on multitemporal satellite imagery and in situ data through machine learning models in Haiyang City during the years 2015 and 2016. The main objectives of this article are as follows.

- 1) To measure the distribution and biomass of the green tide biomass and the respective phytoplankton in the settlement region.
- 2) To explore the relationship between the algae biomass and the marine Chl-a concentrations in the settlement region.
- 3) To analyze the ecological impact pattern and time cycle of the green tide in the settlement region.

II. STUDY AREA AND DATA

A. Study Area

Yellow Sea is a semienclosed shallow sea with an area of about 309 000 km² and is characterized by complex hydrographic conditions [39]. The spatial and temporal distribution of nutrients in the Yellow Sea is highly variable due to the cold, near-shore, and faint currents of the Yangtze River [40]. Haiyang City is located on the northwest Yellow Sea and southeastern coast of the

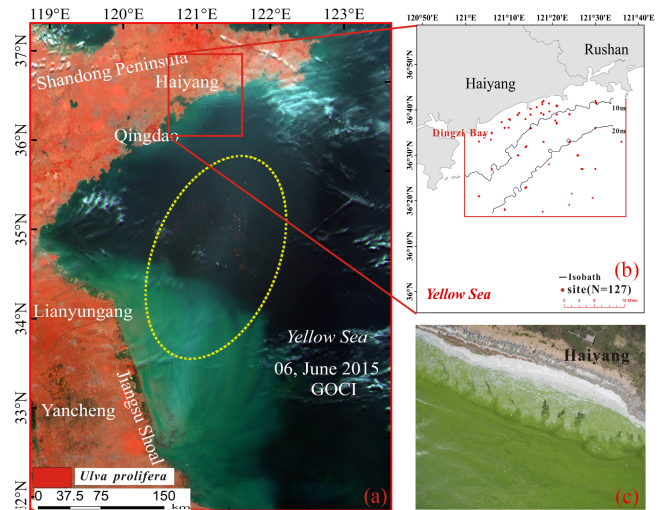


Fig. 1. Map of the study area. (a) Spatial distribution of the green tide recorded on June 6, 2015 (red slicks within the yellow dashed circle) extracted from a GOCI pseudo true color image map of June 6, 2015. Color composites of GOCI bands 865, 555, and 443 nm are coded red, green, and blue, respectively. (b) Distribution map of sampling sites (red dots) in coastal waters south of Haiyang City. Black lines are isobaths and the red frame marks the study area. (c) *U. prolifera* accumulation near the coast of Haiyang City, with dead and decaying *U. prolifera* in white (Google Earth real color imagery).

Shandong Peninsula, near the main settlement region of floating *U. prolifera* (36–36.5° N, 121–124° E). The main reason for the formation of green tides in the region is the strengthening of the southward ocean tides in Shandong Peninsula in July, and the anticyclonic vortex in the southeastern part of Shandong Peninsula [41], [42]. Haiyang city has a temperate maritime climate with the highest rainfall in August, and an annual rainfall of about 190 mm (see Fig. 1) [18]. Furthermore, this area is one of the most important coastal cities in this region, and often under the influence of green tides.

B. Data Used

Remote sensing images with a high temporal resolution are most beneficial for fast-changing phenomena such as green tides. Therefore, Korean GOCI and US MODIS data were selected for this study. GOCI is the world's first geostationary ocean observation satellite launched by Korea. It has 500 m spatial resolution and 1 h temporal resolution. Thus, eight image scenes can be acquired every day. GOCI data are downloaded from the Korean Ocean Satellite Center¹, which also provides processing software [GOCI Data Processing System (GDPS)]. We used GOCI Level-1B and Level-2C data, where the Level-2C data are generated by batch processing of the GDPS. MODIS data are used for auxiliary validation of the green tide biomass model. MODIS Level-0 data of the study area were obtained from the NASA Goddard Space Flight Center (OBPG, <http://oceancolor.gsfc.nasa.gov>). A total of 280 GOCI and 12 MODIS images from May to August for the years 2015 and 2016 have been selected for this study.

¹[Online]. Available: http://kosc.kiost.ac/kosc_web

The GOCI Level-1B data were formatted by GDPS software, and then radiometrically and geometrically corrected using the ENVI software package. All parameters for the radiometric correction were obtained through the GOCI metadata look-up table. The 6S atmospheric correction model was applied to the GOCI imagery to derive the remote sensing reflectance (Rrs) [43]. In this context, an oceanic aerosol type and a midlatitude summer type atmospheric profile embedded in the 6S model were applied [44]. The equations used to calculate the Rrs by the output parameters of the 6S model are as follows:

$$y = x_a * L - x_b$$

$$Rrs = \frac{y}{(1 + y + x_c)} \quad (1)$$

where x_a , x_b , and x_c are the output parameters from the 6S model, L is the apparent radiance, Rrs is the reflectance, and y is the process variable.

Further, GOCI Level-2C data were generated from Level-1B data by batch processing of the GDPS data and represent dimensionless Rayleigh-corrected reflectance (R_{rc}) data.

MODIS Level-0 data were first corrected by removing the molecular (Rayleigh) scattering effects and then converted to R_{rc} through the SeaDAS software

$$R_{rc} = \pi L_t^* / (F_i \cos \theta_i) - R_r \quad (2)$$

where L_t^* is the calibration of sensor radiation after absorption of ozone and other gaseous absorptions, F_i is the extraterrestrial solar irradiance at the time of data collection, θ_i is the solar zenith angle, and R_r is the Rayleigh reflectance.

All GOCI and MODIS R_{rc} data were used for the calculation of the FAI. This article used R_{rc} ratios of two NIR bands and a threshold to mask clouds in GOCI images. Pixels with $R_{rc}_{865 \text{ nm}} > 0.06$ are identified as thick clouds and then masked out. Pixels with $R_{rc}_{865 \text{ nm}} \leq 0.06$, $R_{rc}_{865 \text{ nm}} \geq 0.027$, and $R_{rc}_{745 \text{ nm}} / R_{rc}_{865 \text{ nm}} \leq 1.15$ were also masked [45]. Land masking operations are based on China's coastline data from 2015 to 2016.

C. In Situ Data and Matching-Up

Data collected by a total of 127 sampling stations in Haiyang City include Chl-a concentrations (mg/m^3) and remote sensing reflectance data (Rrs, Sr^{-1}) of the relevant water regions. The data were sampled in May, June, July, and August of 2015 and 2016 (see Table I). June to July is the date when the green tide can be observed floating on the sea surface in the study area.

The water samples were passed through 0.45 μm acetate filters. The filters were first soaked in 1:1000 hydrochloric acid solution for 24 h and then washed in milliQ water to pH neutrality. Phytoplankton cells in water were filtered through GF/F filters and the Chl-a was extracted with 90% (v/v) acetone and measured using a fluorometer (Turner Designs Model 10) [46], [47]. The Chl-a concentration was then determined with the fluorometric method [48].

During the sampling dates in May and August of both years, no MABs were present at the ocean surface in the settlement

TABLE I
RESULTS OF MATCHING THE GOCI DATA WITH THE IN SITU CHL-A IN HAIYANG CITY

Match-Up Dates	No. of Match-Ups	Chl-a (mg/m^3)
		Ave \pm STD
May 10, 2015	10	1.29 \pm 0.40
May 12, 2015	11	1.66 \pm 0.46
May 13, 2015	7	1.59 \pm 0.45
June 27, 2015	9	2.25 \pm 0.51
July 13, 2015	6	2.01 \pm 0.49
August 5, 2015	6	0.62 \pm 0.37
August 7, 2015	6	1.96 \pm 0.46
May 24, 2016	7	1.35 \pm 0.42
May 25, 2016	10	1.47 \pm 0.44
June 25, 2016	10	1.95 \pm 0.48
July 7, 2016	10	2.41 \pm 0.58
August 9, 2016	10	1.65 \pm 0.46
August 10, 2016	11	2.06 \pm 0.51
August 11, 2016	6	1.33 \pm 0.41
August 12, 2016	8	2.21 \pm 0.55
Total	127	1.75 \pm 0.48

region. The sampling sites and their distribution in the study area are to be found in Fig. 1(b).

Rrs(λ) measurements of the sampling stations were obtained with an analytical spectral device called ASD Field-Spec spectroradiometer. The spectral range of the instrument is 350–1050 nm, with a spectral resolution of 1 nm. While using the brightness sensor head should be facing the sea, the zenith angle is 30° from the direction of the nadir and the azimuth angle is 90° from the direction of the sun [49]. By using a standard Halon panel [$L_p(\lambda)$], the upwelling radiance of the water [$L_{tw}(\lambda)$] and the downwelling radiance of the sky [$L_s(\lambda)$] are measured to obtain the Rrs(λ) [50]. The final Rrs(λ) of seawater was calculated for each site by averaging ten measurements each and after removing anomalous spectra. The matching of in situ data with GOCI measurements is completed according to the match-up analysis protocol [51]. Thereby, when at least half of the pixels in the median 3 \times 3 window are valid pixels, they can be used for analysis. The coefficient of variation (calculated as the standard deviation divided by the mean) is <5% within the window. The matching time between GOCI and in situ data allowed for match-up was 1 h. The successfully matched sites are randomly divided into training and testing samples for machine learning according to the ratio of 7:3.

We took the visual interpretation of macroalgae on the image as ground truth because the green algae floating on the water surface has a generally similar spectral property to land vegetation in the visible and near-infrared wavelengths with a typical red-edge signal (700 nm). Considering the physiological characteristics of the green tide and the complex conditions in the ocean, it is difficult to conduct directly measured in situ. Moreover, based on previous research results, macroalgae disasters are often a single species in the study area. Although other algae,

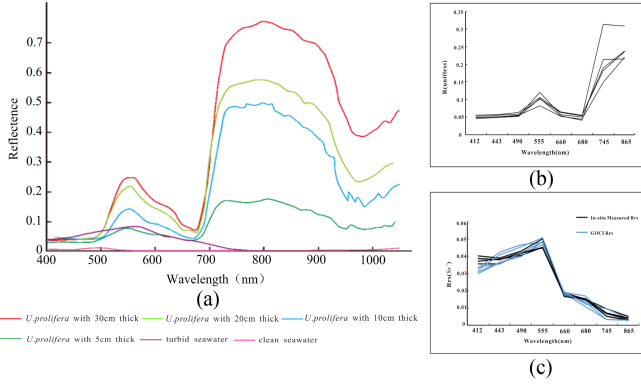


Fig. 2. Spectral reflectance comparison chart. (a) Spectral reflectance of *U. prolifera* and seawater measured in the study area. (b) Spectral reflectance with random pixels of *U. prolifera* corresponding to the eight GOCI bands. (c) Comparison of Rrs of GOCI seawater image pixels with in situ seawater samples in eight bands.

such as *Sargassum*, may be found in some years, the spectral reflectance characteristics of these algae are significantly different [52]. Therefore, the pixels of green algae could be determined by comparing the spectral reflectance characteristics of satellite images and in situ measured *U. prolifera* [see Fig. 2(b)].

The atmospheric calibration results of the GOCI matching points show that the 6S mode has stable performance and high accuracy in the visible band, except for the blue band, the errors between the visible band and the measured data are small [see Fig. 2(c)].

III. METHODS

The key to green tide extraction through remote sensing data is the FAI algorithm, which is used to design the green tide biomass model based on its advantages in mixed-pixel decomposition and sensitivity. Considering the number of match-up data in the study area, the machine learning method for small samples was the choice for this study.

A. Cross-Satellite Biomass Model

The green tide biomass model is obtained based on the FAI (dimensionless), because the FAI is a baseline subtraction algorithm that enables good decomposition of mixed-pixel image and enables cross-satellite calculations with high robustness. The green tide biomass model is an empirical model that was proposed by Hu et al. [53] and is mainly applicable to MODIS images. Considering that GOCI images have a higher temporal resolution than MODIS images, it is necessary to convert the model applicable to MODIS to GOCI images.

The band design of the GOCI instrument is different to that from the MODIS sensor. Thus, the alternative floating algae index (AFAI, similar to FAI but three other bands are used for the linear index) algorithm is chosen to calculate the green tide biomass in GOCI images. The AFAI algorithm is an improved algorithm for the FAI algorithm, which is applicable to images lacking short-wave infrared bands, but the principles of both are the same.

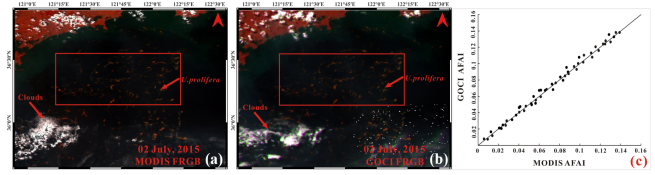


Fig. 3. Comparison of AFAIs between MODIS and GOCI images on July 2, 2015. (a) Spatial distribution of *U. prolifera* (red slicks within the red box) extracted from MODIS false color imagery, $R = R_{rc_859\text{ nm}}$, $G = R_{rc_555\text{ nm}}$, $B = R_{rc_469\text{ nm}}$. (b) Exemplified spatial distribution of *U. prolifera* (red slicks within the red box) extracted from GOCI false color image, $R = R_{rc_865\text{ nm}}$, $G = R_{rc_555\text{ nm}}$, $B = R_{rc_490\text{ nm}}$. (c) Cross correlation of GOCI and MODIS sensor AFAIs of *U. prolifera* pixels.

The AFAI algorithm is a baseline subtraction algorithm, and the formula is as follows:

$$AFAI = R_{NIR} - R'_{NIR} \quad (3)$$

$$R'_{NIR} = R_{RED} + (R_{SWIR} - R_{RED}) \times (\lambda_{NIR} - \lambda_{RED}) / (\lambda_{SWIR} - \lambda_{RED}) \quad (4)$$

where R_{RED} , R_{NIR} , and R_{SWIR} are the R_{rc} of the red, near infrared, and short-wave infrared bands, respectively; λ_{RED} , λ_{NIR} , and λ_{SWIR} are the wavelength of the red, near infrared, and short-wave infrared bands, respectively; and R'_{NIR} is the baseline reflectance. λ_{RED} , λ_{NIR} , and λ_{SWIR} are MODIS bands at 667, 748, and 869 nm, respectively. Adjusted to GOCI, the respective wavebands are 660, 745, and 865 nm [54].

First, the upper limit of the AFAI value at 100% green algae coverage pixels needs to be determined for each sensor. The AFAI value of pixels covered by 100% macroalgae in the MODIS image is about 0.159, whereas the one in the GOCI images from 2015 to 2016 is 0.147 ± 0.002 and 0.143 ± 0.005 , respectively.

The AFAI values calculated by the GOCI sensors were related to the MODIS AFAI (see Fig. 3). Considering the complexity of measuring green tides at sea and the consistency of the timing of the study to the timing of the model validation data of Hu et al. (2017), the green tide biomass model calculated by (5) may be feasible. However, at inshore waters near beaches and shorelines, algae may accumulate with thicker densities than in offshore waters, resulting in the calculated AFAI value > 0.15 . In this case, the biomass of *U. prolifera* in this region will be underestimated by about 40%. Therefore, a buffer zone of 5 km from the shoreline toward the sea was masked when calculating the green tide biomass, whereby, anomalous values of green tide biomass due to accidentally recorded signals from land surfaces are also excluded.

According to the statistical results of the latest study and this article, the upper-bound AFAI threshold value of GOCI imaging was found to be 0.149 [55]. Therefore, the empirical formula for the green tide biomass was modified for our study. The formula is as follows:

$$y = 9x + 0.014 \quad -0.0002 < x \leq 0.149 \quad (5)$$

where x is AFAI (dimensionless) and y is the green tide biomass per area (kg/m^2). AFAI was calculated by using the GOCI L2C product data in the desired band.

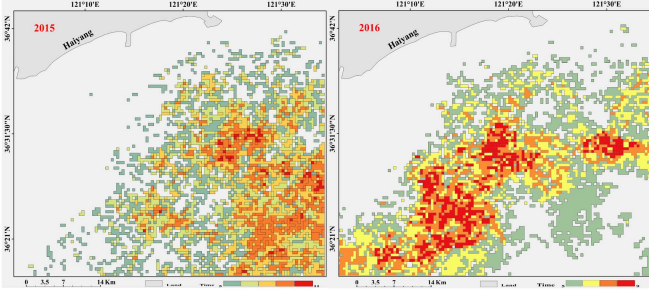


Fig. 4. Regional distribution of HF areas of *U. prolifera* in 2015 and 2016.

B. Pixel-Based Statistics Grid of Green Tides

The green tide in the settlement region is drifted from other regions, whereby the green tide in this region has spatial and temporal differences. In order to investigate the ecological impact of the main areas of the green tide, we counted the pixels with algae cover and marked the areas with five or more occurrences of green tides in all images during the year as high-frequency (HF) areas (see Fig. 4). Moreover, the lasting time of *U. prolifera* that drifted into this region can be calculated by the pixel-based statistics grid of green tides. By comparison, the HF areas of *U. prolifera* were located near the 10 and 20 m isobaths and were concentrated in the southeastern part of the sea in 2015 and in the northwestern part of the sea in 2016. This is highly consistent with the drift directions of the green tides in both years.

C. Support Vector Regression

The SVR method has been proven to perform best in the inversion of Chl-a concentration [56]. The SVR algorithm attempts to find a hyperplane in a high-dimensional space such that all data in the set are closest to that plane [57]. Vapnik introduces an insensitive cost function (ϵ), forming an ϵ -SVR [58]. The SVR formula is as follows:

$$f(\mathbf{x}) = \langle \boldsymbol{\omega}, \mathbf{x} \rangle + b, \boldsymbol{\omega} \in \mathcal{X}, b \in \mathcal{R} \quad (6)$$

where $\langle \cdot, \cdot \rangle$ denotes the dot product, $\boldsymbol{\omega}$ denotes a normal vector of the hyperplane, and b denotes bias parameters.

For the nonlinear problems, this article obtained the SVR model using a nonlinear kernel function, which makes the non-linearly separable problem linearly separable or approximately linearly separable [59], [60]. The function is constructed as

$$K(\mathbf{x}, \mathbf{x}') = \langle \phi(\mathbf{x}), \phi(\mathbf{x}') \rangle \quad (7)$$

where $\phi(\mathbf{x})$ denotes the mapping from the sample to the feature space.

D. Accuracy Assessment

To evaluate the accuracy of the selected machine learning models, the coefficient of determination (R^2), the mean relative error (MRE), and the root-mean-square error (RMSE) between measured and estimated Chl-a was calculated

$$R^2 = \frac{\sum_{i=1}^N (\hat{y}_i - \bar{y})^2}{\sum_{i=1}^N (y_i - \bar{y})^2} \quad (8)$$

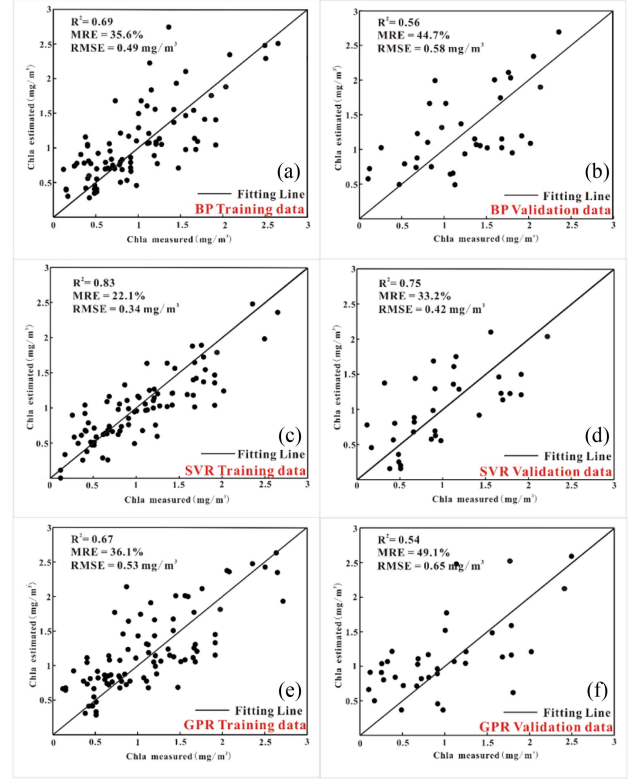


Fig. 5. Performance evaluation of three machine learning models. (a), (c), and (e) represent the training results of the BP, SVR, and GPR models, respectively. (b), (d), and (f) represent the validation results of the BP, SVR, and GPR models, respectively.

$$RMSE = \sqrt{\frac{1}{N} \sum_{i=1}^N (\hat{y}_i - y_i)^2} \quad (9)$$

$$MRE = \frac{1}{N} \sum_{i=1}^N \left| \frac{y_i - \hat{y}_i}{y_i} \right| \times 100\% \quad (10)$$

where y_i and \hat{y}_i are the measured and estimated Chl-a values, respectively, and N is the number of in situ samples.

IV. RESULTS

A. Accuracy Comparison of Machine Learning Models

A total of 127 match-up data from May to August in 2015 and 2016 were randomly divided into training and validation samples with the ratio of 7:3. Models were established using three machine learning algorithms, namely an SVR, a back-propagation neural network (BP), and a Gaussian process regression (GPR). For the respective training samples, the parameters of the three models were continuously optimized, and finally, the accuracy results were obtained (see Fig. 5). These indicate that among the three models, the SVR algorithm showed relatively stable results and higher accuracies (see Table II). The overall accuracy of the SVR model is above 70% and therefore, this model was selected to invert the Chl-a concentrations for the study area.

TABLE II
RESULTS OF THREE MACHINE LEARNING MODELS

	Training data			Validation data		
	R^2	RMSE (mg/m ³)	MRE (%)	R^2	RMSE (mg/m ³)	MRE (%)
SVR	0.83	0.34	22.1	0.75	0.42	33.2
BP	0.69	0.49	35.6	0.56	0.58	44.7
GPR	0.67	0.53	36.1	0.54	0.65	49.1

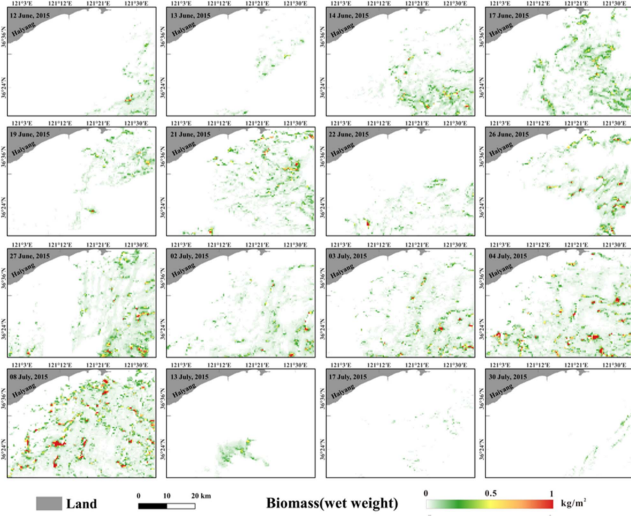


Fig. 6. Distribution of the green tide biomass in the study area in 2015.

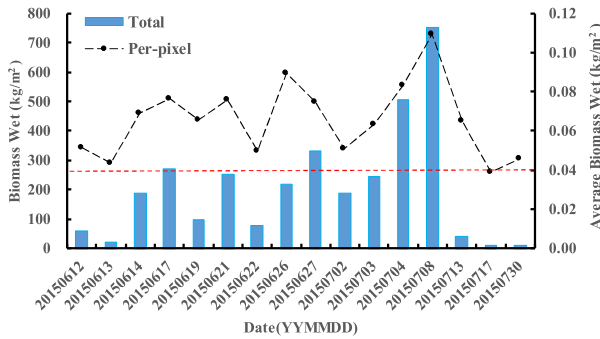


Fig. 7. Statistical chart of the total biomass and the per-pixel averaged biomass of the green tide in 2015. The red dashed line represents the lowest per-pixel average of the biomass.

B. Spatio–Temporal Distribution of the Green Tide Biomass

Through the green tide biomass model, we obtained the *U. prolifera* biomass statistics and distribution map in the study region between 2015 and 2016 (see Figs. 6–9). In 2015, the earliest intrusion of algae was discovered by GOCI data on June 12. The green tide was initially located in the southeast of the study region, with a total wet weight of about 60.68 kg/m². The last date of occurrence of the green algae in 2015 was monitored at July 17, but a remaining part of the green tide stayed distributed till July 30, due to the influence of winds

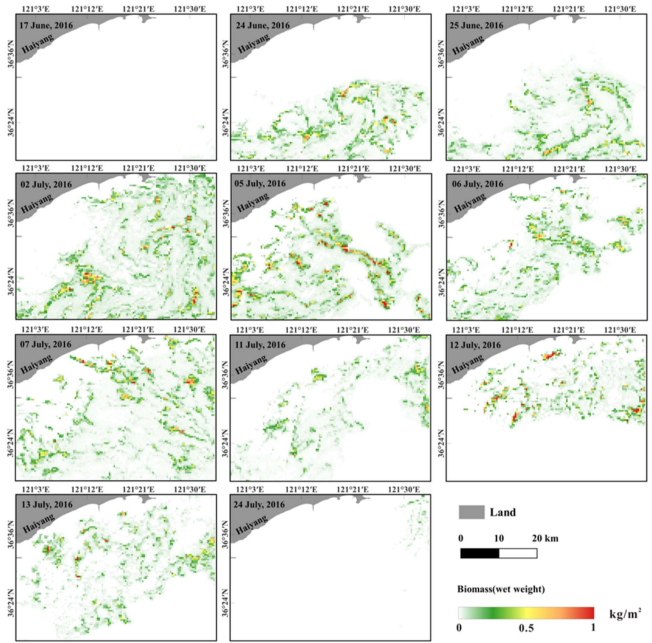


Fig. 8. Distribution of the green tide biomass in the study area in 2016.

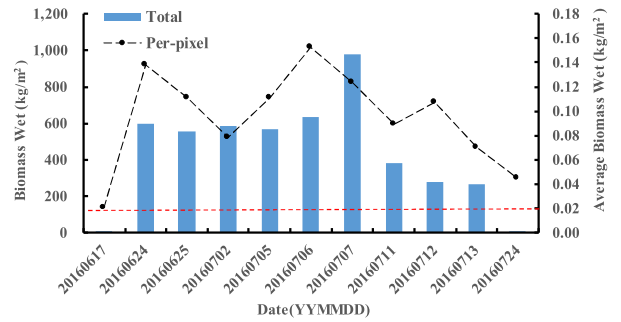


Fig. 9. Statistical chart of the total biomass and the per-pixel averaged biomass of the green tide in 2016. The red dashed line represents the lowest per-pixel average of the biomass.

and sea surface currents. Results revealed that from June 12 to July 8, the total biomass of the green tide showed an overall increasing trend. On July 8 the total biomass of the intruded green tide reached its maximum with 751.62 kg/m². During this period, *U. prolifera* gradually drifted from the southeast to the inshore waters of Haiyang City in the northwest. After July 8, the total biomass began to decrease significantly, and the distribution range was reduced to the southern part of Haiyang City. On July 17, the total biomass reached about 9.99 kg/m². On July 30, a smaller part of algae floated in the study area, where the total biomass was about 11.51 kg/m². Although the frequent rise of thin clouds often prevented daily observations, the results show an overall increasing trend in 2015 between June 12 and June 26. The average per-pixel biomass values on June 26 and July 8 were similar (0.09 and 0.11 kg/m², respectively), and developed two major peaks during the year. During this period, the average biomass first decreased and later increased. This indicates the occurrence of two peaks of the biomass in the

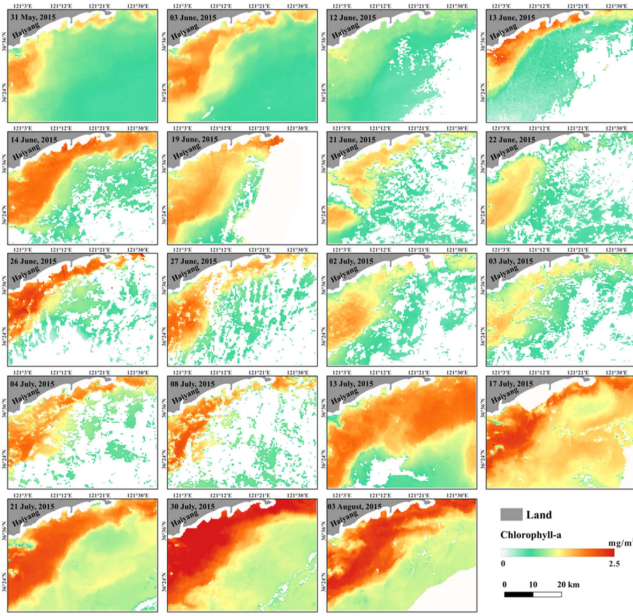


Fig. 10. Distribution of marine Chl-a concentrations in 2015.

study area from the emergence till the decomposition of the green tide.

In 2016, the earliest intrusion of green tides was discovered on June 17, which was delayed compared to the initial detection date in 2015. It was found that small patches of green algae were scattered and arranged in the southeastern part of the study region on June 17, with a total biomass of about 1.69 kg/m². On June 24, it was observed that large-scale green algae were distributed in the southern part of Haiyang City, with a relatively high biomass of about 598.68 kg/m². Due to a high cloud coverage, there were no GOCI images available in the study area between June 17 and 24. In contrast to 2015, the total biomass of the green tide in 2016 showed a trend of strong increase in the beginning of the emergence, followed by a constant decrease toward its decomposition. July 7 marked the day with the highest amount of biomass in this year at about 978.06 kg/m². On that day, massive green tides were distributed in the entire study area. Further large-scale green tides occurred on July 2, and the biomass in the sea near Haiyang City remained at a high level until July 11. According to the satellite time-series results, the decomposition period of the macroalgae in the study area in 2016 was between July 13 and 24.

C. Spatio-Temporal Distribution of the Chl-a Concentration

The SVR neural network method was further used to derive the spatial-temporal distribution of Chl-a concentrations (see Figs. 10 and 11) and to calculate the daily average marine Chl-a concentrations in the settlement region (see Figs. 12 and 13). In this case, the much stronger spectral Chl-a response of the green macroalgae pixels in contrast to the phytoplankton in the ocean needs to be masked during the inversion. The Chl-a concentration varied drastically at the Dingzi Bay in the study area, this would have an impact on the analysis of the relationship

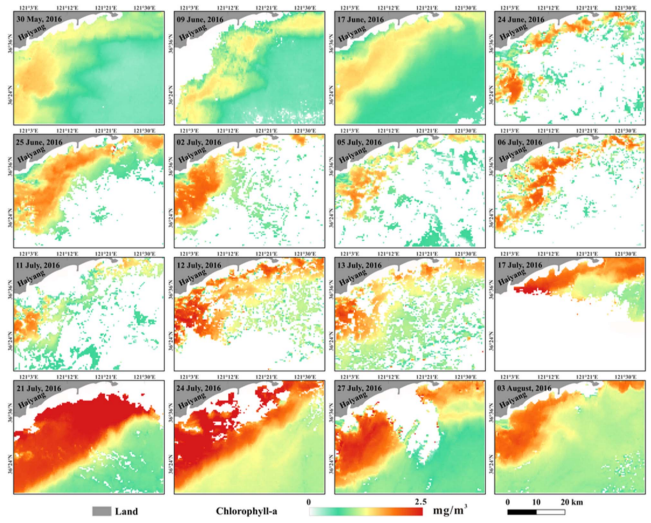


Fig. 11. Distribution of marine Chl-a concentrations in 2016.

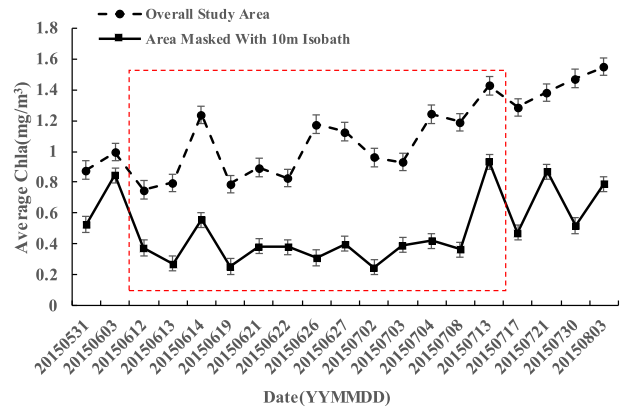


Fig. 12. Statistical chart of average marine Chl-a concentrations in 2015. The red dashed box encompasses the time frame during which *U. prolifera* occurred in the study area.

between green tide biomass and marine Chl-a concentration. Therefore, the area <10 m isobath is masked in this article [61].

The results show that from the end of May to June 12, 2015 (before the first acquisition of green tides by the satellite), the Chl-a concentrations in the southeastern part of the settlement region were increased. From June 12 to July 13, the Chl-a concentrations of seawater pixels with no-algae showed a decreasing trend. From July 17, when the macroalgae started to decompose, the concentration of marine Chl-a in the Haiyang City increased. The overall Chl-a concentration in the study area before masking showed an increasing trend as compared to the results after masking, whereas the results after masking were more stable (see Fig. 12).

In 2016, from June 17 to July 13, the overall concentration of marine Chl-a after masking showed a decreasing trend in the study area. According to the statistical results of green tide grid, it was found that there was a higher occurrence of macroalgae near the 10 and 20 m isobaths (see Fig. 4). After July 21, the Chl-a concentration began to decrease. At the end

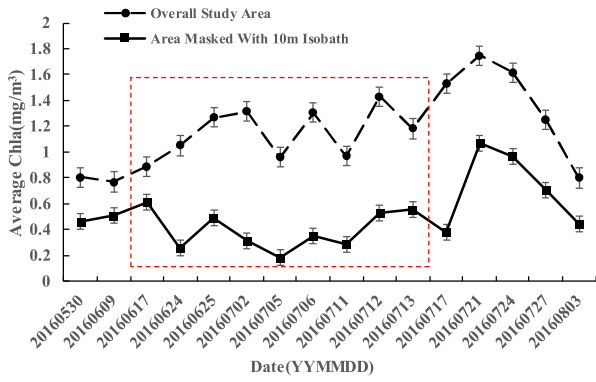


Fig. 13. Statistical chart of average marine Chl-a concentrations in 2016. The red dashed box encompasses the time frame during which *U. prolifera* occurred in the study area.

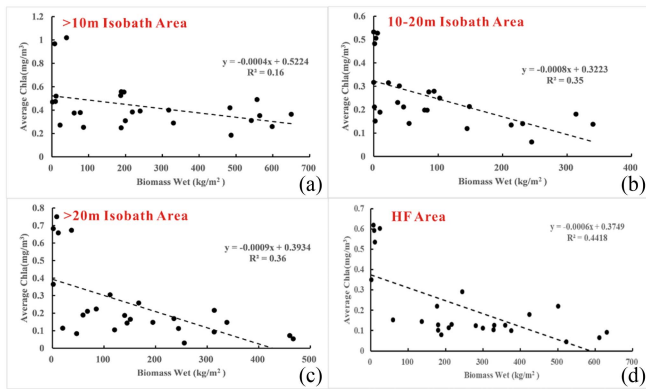


Fig. 14. Correlations between green tide biomass and Chl-a concentrations in different regions during two years. (a) >10 m isobath area. (b) 10–20 m isobath area. (c) >20 m isobath area. (d) HF area.

of May and in the beginning of August, the Chl-a concentration in the study area remained at a stable level between the two dates (the concentrations of marine Chl-a were 0.46 and 0.44 mg/m³, respectively) (see Fig. 13).

V. DISCUSSION

A. Ecological Impact Patterns of Green Tides Biomass in the Settlement Region

After masking the river inlet and land area, this article found that the Chl-a concentration in the observed sea area was maintained at a low level during the presence of the green tide, and the Chl-a concentration was negatively correlated with the green tide biomass (see Figs. 12–14). When the green tides biomass increased, the Chl-a concentration in the corresponding area began to decrease. This relationship is most evident in the HF areas.

Based on the correlation results, the variation patterns within the marine Chl-a during the process from the emergence to the decomposition of *U. prolifera* in the settlement region were further analyzed (see Figs. 15 and 16).

The growth rate of marine surface phytoplankton is regulated by temperature, light, nutrients, and many other environmental

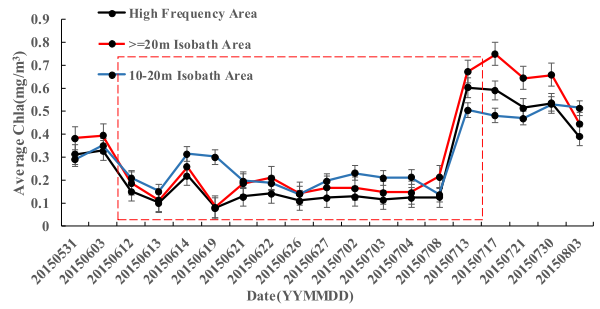


Fig. 15. Statistical chart of Chl-a concentrations for different regions in the study area in 2015. The red dashed box encompasses the time frame during which *U. prolifera* occurred in the study area.

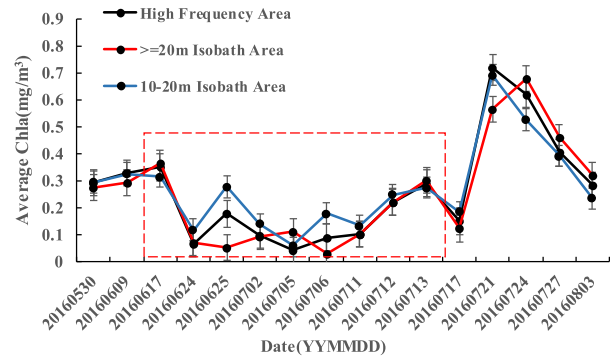


Fig. 16. Statistical chart of Chl-a concentrations for different regions in the study area in 2016. The red dashed box encompasses the time frame during which *U. prolifera* occurred in the study area.

factors [62], [63]. However, during the existence of the green tide, *U. prolifera* is the dominant species, which severely inhibits the growth of phytoplankton, and environmental factors mainly affect the green tide algae [64], [65], [66].

During the initial stage of the green tide in the settlement region, algae floating on the surface absorbed abundant nutrients and block sunlight from reaching deeper layers, thus inhibiting the growth and reproduction of phytoplankton, and eventually leading to a decline in Chl-a in the corresponding sea area [64], [67]. Thereafter, the Chl-a concentrations in different regions showed a “valley bottom,” which is consistent with the high macroalgae biomass area. In particular, as the floating green tide drifts, Chl-a concentrations fluctuate between different regions, such as on June 24 and 25, 2016. Plankton growth is restored in the region after the green tide has drifted [68]. Then, although the MABs distribution changed, the phytoplankton production was still inhibited. Finally, the Chl-a concentration starts to rebound at the decomposition of the green tide. The decay and decomposition of the green macroalgae release large amounts of nutrients, thereby aggravating the eutrophication of the relevant area [15], [69]. At the same time, the disappearance of the green tide will alleviate its inhibitory effect on the phytoplankton, which allows it to recover [34], [70].

The study area is primarily influenced by the Yellow Sea Coastal Current during the summer season. After removing the estuary area, we further analyzed the influence of currents on marine Chl-a concentration by using salinity and currents data

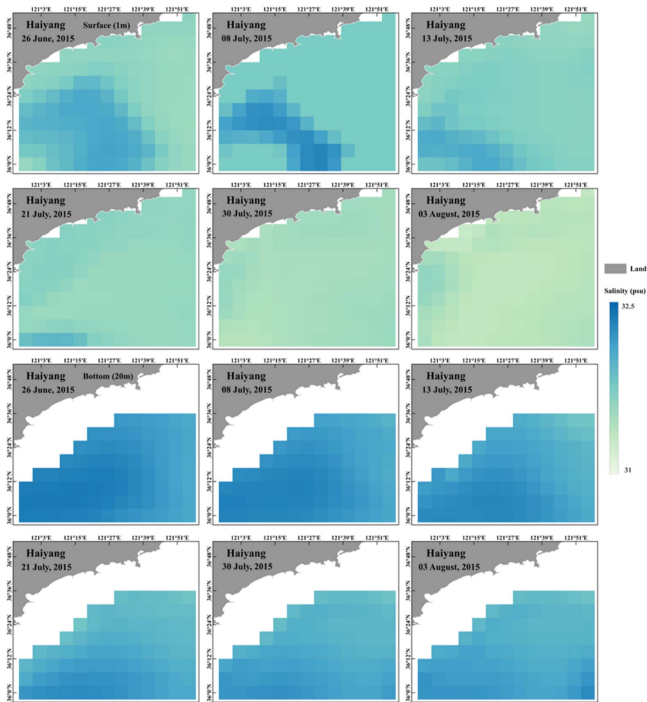


Fig. 17. Spatial distribution of surface (1 m) and bottom (20 m) salinity in the study area in 2015.

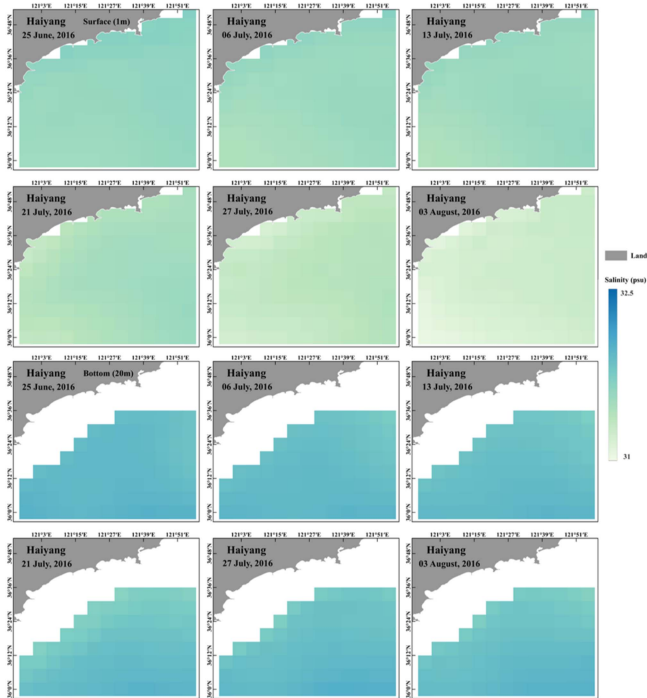


Fig. 18. Spatial distribution of surface (1 m) and bottom (20 m) salinity in the study area in 2016.

(see Figs. 17–19). Salinity and currents data were obtained from the Global Ocean Forecasting System.² Through the results of salinity and currents, it was found that from late May to early August in both years, the study area was mainly influenced

²[Online]. Available: <https://www.hycom.org/dataserver/gofs-3pt1/analysis>

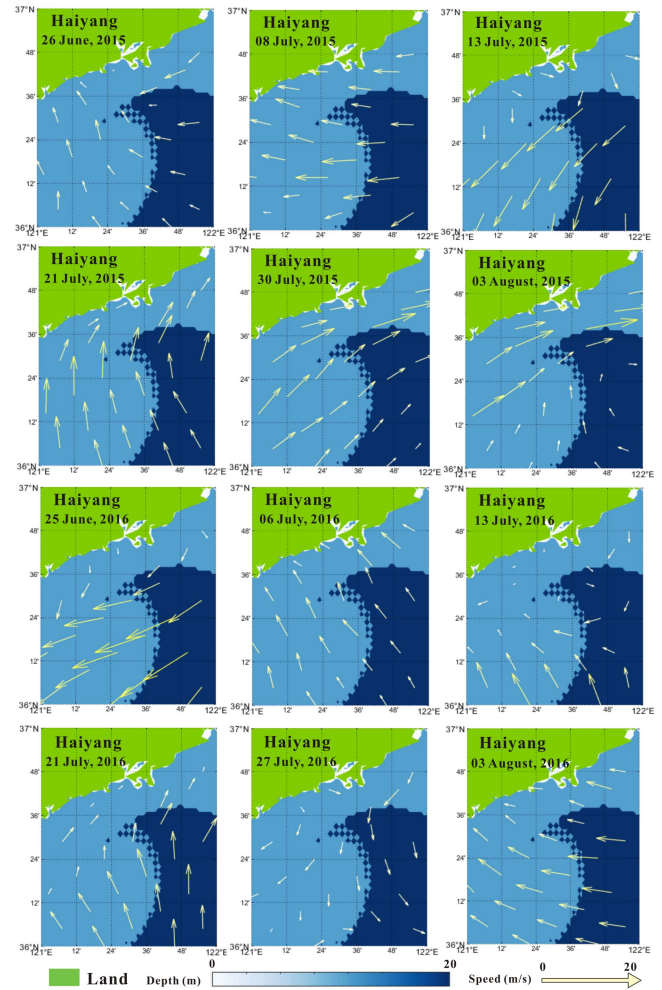


Fig. 19. Surface currents in the study area for the years 2015 and 2016.

by northwestward coastal currents, with relatively stable flow velocities and minor variations in surface and bottom salinity. On July 8th, 2015, the southwestern part of the study area exhibited the highest surface salinity, reaching approximately 32.1 psu. This can be attributed to the passage of a typhoon in early July. During a typhoon event, surface salinity tends to increase due to vertical mixing and enhanced wave breaking, which reduces the water transparency due to reduced sunlight availability [71]. In addition, typhoons also reduce sea surface temperature, which will limit the growth of Chl-a concentration to some extent [72]. In comparison, the salinity distribution in the study area was relatively stable in 2016.

Based on the recorded variations in the concentration of satellite-derived Chl-a in the Yellow Sea over the past 20 years, it was determined that the southeastern region of the Shandong Peninsula had the lowest Chl-a concentration in summer, with a value of approximately 0.7 mg/m^3 [73]. The average Chl-a concentration from remote sensing satellites and samples measurement during the months of June and July in years without green tides is approximately 1.1 mg/m^3 (see Fig. 20) [74], [75]. This indicates that the Chl-a concentration in the year without green tides was much higher than that in the year when green tides occur [33]. Meanwhile, these results are significantly higher

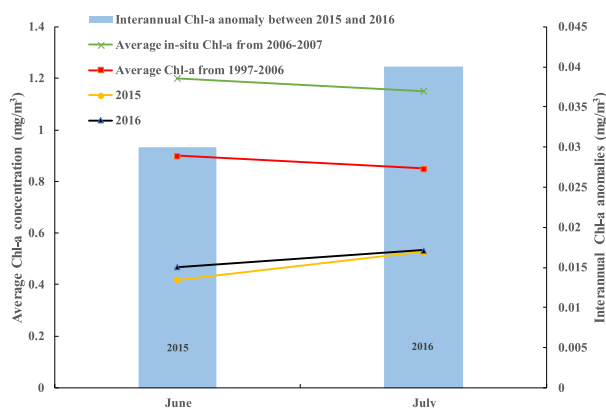


Fig. 20. Comparison of average Chl-a concentrations in the study area for June and July. The red line in the graph represents the 10-year average trend of no green tide occurrence extracted from remote sensing data [74]; the green line represents the average trend of measured Chl-a concentration in 2006–2007 [75]; the black and yellow lines represent the average trends of Chl-a concentrations in this study measured for 2105 and 2016, respectively; the blue bars represent the interannual Chl-a anomalies in 2015 and 2016 [76].

than the minimum Chl-a concentration during the occurrence of green tides in this article (0.1 mg/m^3). When considering the average trends in Chl-a concentration over 20 and 10 years, it is evident that the summer Chl-a concentration remains stable, with minimal influence from ocean currents. The main factors contributing to the variations in Chl-a concentration in the region are green tides in combination with some special conditions (such as typhoons).

In general, the ecological impact patterns in the settlement region reveal a decreasing trend of the Chl-a concentrations with the increase in green tide biomass. However, there was a limit to this trend, when the lowest value of Chl-a concentration was maintained at $0.1\text{--}0.2 \text{ mg/m}^3$. After the decomposition of the *U. prolifera*, the Chl-a in the settlement region increased strongly, and when the concentration reached about $0.7\text{--}0.8 \text{ mg/m}^3$, it began to gradually decrease.

B. Green Tides Temporal Cycle in the Settlement Region

The low nutrient content and the high sea surface temperatures in the ocean near Haiyang City are not suitable for the growth and reproduction of algae as compared to the area of origin and thus, the settlement region is a place for natural decay and decomposition of green tides [77], [78], [79]. When the green algae in the Yellow Sea drifted to the waters near Haiyang City in the Shandong Province, it already entered the decline stage, indicated by the short duration and rapid decrease in total biomass [13], [35]. Although the green tide biomass in the study area showed a gradually increasing trend, the monitoring results based on multitemporal satellite data revealed that it was related to the large-scale MABs drift from the Yellow Sea [6].

Our investigations show that the residence time of the green tide in the settlement region was short and the overall biomass declined rapidly during the two years (see Figs. 6 and 8). Through the statistics of time-series remote sensing data, the longest dwelling time of green tides that existed in the settlement region was about 30 d in both years. Certainly, this finding is only

based on statistical results of remote sensing data with frequent cloud cover and strong sun glint; there is no guarantee that data on continuous time-series are available. The analysis based on the average Chl-a concentration shows that this time cycle lasts about 35 d. Therefore, combining the existence period of green tides with the statistical results of average Chl-a concentration, the temporal cycle of green tides in the settlement region is about 30–35 d. Still, the green tide decay and decomposition process in the settlement region is continuous and dramatic [55], [80]. It is worth noting that this period is influenced by the amount and frequency of green tide biomasses that drift into the settlement region.

C. Special Cases

The difference in the patterns of the green tide in the settlement region between 2015 and 2016 revealed that typhoons can have a significant impact on the ecological environment in two main ways.

First, it changes the temporal cycle of green tides. Comparing the high temporal resolution data of the GOCI and MODIS sensors, with the green tide biomass and the information from related studies, it is obvious that in 2015 two green tide appearances occurred, which is consistent with the drift of MABs from the Yellow Sea during this year [11]. Around June 27, 2015, a massive green tide originating from the Yellow Sea drifted toward the waters near the study area driven by surface winds and currents [61], [81]. At the same time, the center of the green tide bloom began to drift in a southwesterly direction, which was in contrast to the overall drift direction in June. Under the influence of typhoon “Chan-hom,” the floating algae drifted into the study area once again resulting in an increase in the overall green tide biomass on July 2, 2015 [61]. The increased frequency of green tides drifting into the settlement region prolonged the temporal cycle to about 35 d in 2015. In 2016, only one large-scale green tide drifted into the study area in contrast to 2015 [16], [82], [83].

Second, after the passage of typhoons, there is an impact on the ecological environment of the settlement area. In Section V-A, this article revealed that the passage of the typhoon intensified the trend of low Chl-a concentrations in the study area. Additionally, around July 13th, 2015, when the typhoon departed from the Yellow Sea, the concentration of Chl-a in the settlement region remained at a high level. The difference to 2015 is that the increase in Chl-a in 2016 did not last for a long time and began to decline significantly after reaching the peak. Some studies indicated that the vertical mixing of seawater caused by the typhoon in July 2015 provided rich nutrients. This leads to high concentrations of Chl-a in the passage of the typhoon [84].

D. Prospect

In response to the ecological impacts of green tides in the settlement region, this article has conducted corresponding research. We found further ecological patterns of green tides within the settlement region that need more detailed in-depth studies.

The settlement region serves as a critical area for the natural decay and decomposition of green tide, and it has obvious ecological consequences. Haiyang City is a major coastal region frequently infested by the green tide disaster every year. It is also an important area for studying the ecological impacts of green tide within the settlement region. Although this study area is relatively small, it experiences fewer natural and anthropogenic disturbance factors than other regions, making it universally applicable and representative for investigating the ecological consequences of green tides.

Due to the nature of green tide disasters, there is limited publicly available sample data on seawater quality during the decay and decomposition processes of green tides. Meanwhile, fewer remote sensing data products of marine Chl-a (such as MODIS and GOCI Chl-a concentration daily data) are available. In addition, machine learning is a suitable tool for providing a good performance even for small sample training data. Therefore, we chose a machine learning algorithm rather than a deep learning one for the inversion of marine Chl-a concentrations. Thereby, in future research, we further intend to create and produce publicly remote sensing datasets for the green tide in the settlement region.

VI. CONCLUSION

In this article, we investigated the ecological impact patterns of the green tide biomass during the years 2015 and 2016 in Haiyang City, Shandong Province, China, and the main settlement region of *U. prolifera*. Results show that the SVR machine learning model is more suitable for the inversion of Chl-a concentrations in the study area. Our research shows that the biomass of green tides has a significant negative correlation on the concentrations of Chl-a in the settlement region. The Chl-a concentration showed a decreasing trend and remained at a low level (0.1–0.2 mg/m³) when the biomass of the green tide increased. With the decomposition of the green tide, the Chl-a in the HF regions accreted rapidly with a peak at about 0.7 mg/m³, and then began to gradually decrease. This article found the temporal cycle of green tides in the settlement region is about 30–35 d, whereby special events, such as typhoons, can influence the pattern and temporal cycle. Furthermore, decay and decomposition of green tides can trigger marine eutrophication with significant ecological consequences in the settlement region.

In general, ecological change patterns of green tides need urgent attention in the settlement region. Therefore, it is recommended to strengthen the interregional cooperation, salvage and clean-up of the green tide in time, and to provide further scientific support for the continuous monitoring of the marine ecological environment.

REFERENCES

- [1] M. Wang and C. Hu, "Mapping and quantifying Sargassum distribution and coverage in the Central West Atlantic using MODIS observations," *Remote Sens. Environ.*, vol. 183, pp. 350–367, 2016.
- [2] R. Bermejo et al., "Spatial and temporal variability of biomass and composition of green tides in Ireland," *Harmful Algae*, vol. 81, pp. 94–105, 2019.
- [3] E. Berdalet et al., "GlobalHAB: A new program to promote international research, observations, and modeling of harmful algal blooms in aquatic systems," *Oceanography*, vol. 30, no. 1, pp. 70–81, 2017.
- [4] D. Liu, J. K. Keesing, Q. Xing, and P. Shi, "World's largest macroalgal bloom caused by expansion of seaweed aquaculture in China," *Mar. Pollut. Bull.*, vol. 58, no. 6, pp. 888–895, 2009.
- [5] Q. Xing et al., "World's largest macroalgal blooms altered phytoplankton biomass in summer in the Yellow Sea: Satellite observations," *Remote Sens.*, vol. 7, no. 9, pp. 12297–12313, 2015.
- [6] G. Zhang et al., "Adaptive threshold model in Google Earth Engine: A case study of *Ulva prolifera* extraction in the South Yellow Sea, China," *Remote Sens.*, vol. 13, no. 16, 2021, Art. no. 3240.
- [7] G. Gao, Z. Zhong, X. Zhou, and J. Xu, "Changes in morphological plasticity of *Ulva prolifera* under different environmental conditions: A laboratory experiment," *Harmful Algae*, vol. 59, pp. 51–58, 2016.
- [8] G. Gao, A. S. Clare, C. Rose, and G. S. Caldwell, "Intrinsic and extrinsic control of reproduction in the green tide-forming alga, *Ulva rigida*," *Environ. Exp. Botany*, vol. 139, pp. 14–22, 2017.
- [9] Q.-C. Zhang et al., "Application of a fluorescence in situ hybridization (FISH) method to study green tides in the Yellow Sea," *Estuarine, Coastal Shelf Sci.*, vol. 163, pp. 112–119, 2015.
- [10] Y. Z. Tang and C. J. Gobler, "The green macroalga, *Ulva lactuca*, inhibits the growth of seven common harmful algal bloom species via allelopathy," *Harmful Algae*, vol. 10, no. 5, pp. 480–488, 2011.
- [11] X. Sun et al., "Spatio-temporal patterns of *Ulva prolifera* blooms and the corresponding influence on chlorophyll-a concentration in the Southern Yellow Sea, China," *Sci. Total Environ.*, vol. 640, pp. 807–820, 2018.
- [12] Y. Zhang et al., "*Ulva prolifera* green-tide outbreaks and their environmental impact in the Yellow Sea, China," *Nat. Sci. Rev.*, vol. 6, pp. 825–838, 2019.
- [13] H. Zhang, G. Wang, C. Zhang, R. Su, X. Shi, and X. Wang, "Characterization of the development stages and roles of nutrients and other environmental factors in green tides in the Southern Yellow Sea, China," *Harmful Algae*, vol. 98, 2020, Art. no. 101893.
- [14] M. Gladyshev and Y. I. Gubelit, "Green tides: New consequences of the eutrophication of natural waters (invited review)," *Contemp. Problems Ecol.*, vol. 12, no. 2, pp. 109–125, 2019.
- [15] P. M. Glibert, "Eutrophication, harmful algae and biodiversity—Challenging paradigms in a world of complex nutrient changes," *Mar. Pollut. Bull.*, vol. 124, no. 2, pp. 591–606, 2017.
- [16] Q. Xing and C. Hu, "Mapping macroalgal blooms in the Yellow Sea and East China Sea using HJ-1 and Landsat data: Application of a virtual baseline reflectance height technique," *Remote Sens. Environ.*, vol. 178, pp. 113–126, 2016.
- [17] W. Shi and M. Wang, "Green macroalgal blooms in the Yellow Sea during the spring and summer of 2008," *J. Geophys. Res., Oceans*, vol. 114, no. C12, 2009, Art. no. C12010.
- [18] L. Zheng et al., "What causes the great green tide disaster in the South Yellow Sea of China in 2021?," *Ecol. Indicators*, vol. 140, 2022, Art. no. 108988.
- [19] C. Hu, "A novel ocean color index to detect floating algae in the global oceans," *Remote Sens. Environ.*, vol. 113, no. 10, pp. 2118–2129, 2009.
- [20] E. T. Harvey, S. Kratzer, and P. Philipson, "Satellite-based water quality monitoring for improved spatial and temporal retrieval of chlorophyll-a in coastal waters," *Remote Sens. Environ.*, vol. 158, pp. 417–430, 2015.
- [21] R. J. Brewin, D. E. Raitsos, Y. Pradhan, and I. Hoteit, "Comparison of chlorophyll in the Red Sea derived from MODIS-Aqua and in vivo fluorescence," *Remote Sens. Environ.*, vol. 136, pp. 218–224, 2013.
- [22] G. Zibordi, J.-F. Berthon, F. Mélin, and D. D'Alimonte, "Cross-site consistent in situ measurements for satellite ocean color applications: The BiOMAP radiometric dataset," *Remote Sens. Environ.*, vol. 115, no. 8, pp. 2104–2115, 2011.
- [23] C. Hu, Z. Lee, and B. Franz, "Chlorophyll-a algorithms for oligotrophic oceans: A novel approach based on three-band reflectance difference," *J. Geophys. Res., Oceans*, vol. 117, no. C1, 2012, Art. no. C01011.
- [24] J. E. O'Reilly et al., "Ocean color chlorophyll algorithms for SeaWiFS," *J. Geophys. Res., Oceans*, vol. 103, no. C11, pp. 24937–24953, 1998.
- [25] Z. Lee, R. Arnone, C. Hu, P. J. Werdell, and B. Lubac, "Uncertainties of optical parameters and their propagations in an analytical ocean color inversion algorithm," *Appl. Opt.*, vol. 49, no. 3, pp. 369–381, 2010.
- [26] J. He, Y. Chen, J. Wu, D. A. Stow, and G. Christakos, "Space-time chlorophyll-a retrieval in optically complex waters that accounts for remote sensing and modeling uncertainties and improves remote estimation accuracy," *Water Res.*, vol. 171, 2020, Art. no. 115403.

- [27] K. Stamnes et al., "Accurate and self-consistent ocean color algorithm: Simultaneous retrieval of aerosol optical properties and chlorophyll concentrations," *Appl. Opt.*, vol. 42, no. 6, pp. 939–951, 2003.
- [28] C. Hu, L. Feng, and Q. Guan, "A machine learning approach to estimate surface chlorophyll a concentrations in global oceans from satellite measurements," *IEEE Trans. Geosci. Remote Sens.*, vol. 59, no. 6, pp. 4590–4607, Jun. 2021.
- [29] C. Wang, R.-C. Yu, and M.-J. Zhou, "Effects of the decomposing green macroalga *Ulva (Enteromorpha) prolifera* on the growth of four red-tide species," *Harmful Algae*, vol. 16, pp. 12–19, 2012.
- [30] B. Huang, N. Wei, J. Tang, and Y. Jin, "Changes of phytoplankton community structure and diversity in the South Yellow Sea during 2007–2017," *Environ. Monit. China*, vol. 34, no. 6, pp. 137–148, 2018.
- [31] K. Sun et al., "A numerical study of the *Ulva prolifera* biomass during the green tides in China—Toward a cleaner *Porphyra* mariculture," *Mar. Pollut. Bull.*, vol. 161, 2020, Art. no. 111805.
- [32] L. Qi, C. Hu, Q. Xing, and S. Shang, "Long-term trend of *Ulva prolifera* blooms in the western Yellow Sea," *Harmful Algae*, vol. 58, pp. 35–44, 2016.
- [33] D. Li, Z. Gao, and Y. Wang, "Research on the long-term relationship between green tide and chlorophyll-a concentration in the Yellow Sea based on Google Earth Engine," *Mar. Pollut. Bull.*, vol. 177, 2022, Art. no. 113574.
- [34] J.-Y. Zhao et al., "Green tides in the Yellow Sea promoted the proliferation of pelagophyte *Aureococcus anophagefferens*," *Environ. Sci. Technol.*, vol. 56, no. 5, pp. 3056–3064, 2022.
- [35] H. Geng, R. Yu, Q. Zhang, T. Yan, F. Kong, and M. Zhou, "Tracing the settlement region of massive floating green algae in the Yellow Sea," *J. Oceanol. Limnol.*, vol. 37, no. 5, pp. 1555–1565, 2019.
- [36] X. Miao et al., "Distribution and species diversity of the floating green macroalgae and micro-propagules in the Subei Shoal, southwestern Yellow Sea," *PeerJ*, vol. 8, 2020, Art. no. e10538.
- [37] D. A. Lyons et al., "Macroalgal blooms alter community structure and primary productivity in marine ecosystems," *Glob. Change Biol.*, vol. 20, no. 9, pp. 2712–2724, 2014.
- [38] B. Wang, M. Xin, Q. Wei, and L. Xie, "A historical overview of coastal eutrophication in the China Seas," *Mar. Pollut. Bull.*, vol. 136, pp. 394–400, 2018.
- [39] C. Liu et al., "Variability in phytoplankton biomass and effects of sea surface temperature based on satellite data from the Yellow Sea, China," *Plos One*, vol. 14, no. 8, 2019, Art. no. e0220058.
- [40] Y. Zhou, L. Tan, Q. Pang, F. Li, and J. Wang, "Influence of nutrients pollution on the growth and organic matter output of *Ulva prolifera* in the southern Yellow Sea, China," *Mar. Pollut. Bull.*, vol. 95, no. 1, pp. 107–114, 2015.
- [41] X. Shi, S. Shen, H.-i. Yi, Z. Chen, and Y. Meng, "Modern sedimentary environments and dynamic depositional systems in the southern Yellow Sea," *Chin. Sci. Bull.*, vol. 48, pp. 1–7, 2003.
- [42] D. Yang, B. Yin, Z. Liu, T. Bai, J. Qi, and H. Chen, "Numerical study on the pattern and origins of Kuroshio branches in the bottom water of southern East China Sea in summer," *J. Geophys. Res., Oceans*, vol. 117, no. C2, 2012, Art. no. C02014.
- [43] E. F. Vermote, D. Tanré, J. L. Deuze, M. Herman, and J.-J. Morcette, "Second simulation of the satellite signal in the solar spectrum, 6S: An overview," *IEEE Trans. Geosci. Remote Sens.*, vol. 35, no. 3, pp. 675–686, May 1997.
- [44] C. Huang et al., "Satellite observation of hourly dynamic characteristics of algae with Geostationary Ocean Color Imager (GOCI) data in Lake Taihu," *Remote Sens. Environ.*, vol. 159, pp. 278–287, 2015.
- [45] M. Wang and W. Shi, "Cloud masking for ocean color data processing in the coastal regions," *IEEE Trans. Geosci. Remote Sens.*, vol. 44, no. 11, pp. 3196–3105, Nov. 2006.
- [46] W. Zhou, X. Yuan, W. Huo, and K. Yin, "Distribution of chlorophyll a and primary productivity in the adjacent sea area of Changjiang River Estuary," *Acta Oceanologica Sin.*, vol. 26, no. 3, pp. 143–150, 2004.
- [47] Z.-X. Zhou, R.-C. Yu, and M.-J. Zhou, "Resolving the complex relationship between harmful algal blooms and environmental factors in the coastal waters adjacent to the Changjiang River estuary," *Harmful Algae*, vol. 62, pp. 60–72, 2017.
- [48] W. Chen, "Discussion on possible error for phytoplankton chlorophyll- α concentration analysis using hot-ethanol extraction method," *J. Lake Sci.*, vol. 18, pp. 550–552, 2006.
- [49] Q. Xing et al., "Monitoring seaweed aquaculture in the Yellow Sea with multiple sensors for managing the disaster of macroalgal blooms," *Remote Sens. Environ.*, vol. 231, 2019, Art. no. 111279.
- [50] C.-C. Huang, Y.-M. Li, D.-Y. Sun, and C.-F. Le, "Retrieval of *Microcystis* aetginosa percentage from high turbid and eutrophication inland water: A case study in Taihu Lake," *IEEE Trans. Geosci. Remote Sens.*, vol. 49, no. 10, pp. 4090–4100, Oct. 2011.
- [51] P. J. Werdell and S. W. Bailey, "An improved in-situ bio-optical data set for ocean color algorithm development and satellite data product validation," *Remote Sens. Environ.*, vol. 98, no. 1, pp. 122–140, 2005.
- [52] L. Qi and C. Hu, "To what extent can *Ulva* and *Sargassum* be detected and separated in satellite imagery?," *Harmful Algae*, vol. 103, 2021, Art. no. 102001.
- [53] L. Hu, C. Hu, and H. Ming-Xia, "Remote estimation of biomass of *Ulva prolifera* macroalgae in the Yellow Sea," *Remote Sens. Environ.*, vol. 192, pp. 217–227, 2017.
- [54] L. Qi, C. Hu, M. Wang, S. Shang, and C. Wilson, "Floating algae blooms in the East China Sea," *Geophys. Res. Lett.*, vol. 44, no. 22, pp. 11501–11509, 2017.
- [55] C. Hu et al., "Mapping *Ulva prolifera* green tides from space: A revisit on algorithm design and data products," *Int. J. Appl. Earth Observ. Geoinf.*, vol. 116, 2023, Art. no. 103173.
- [56] A. Mora-Soto et al., "A high-resolution global map of giant kelp (*Macrocystis pyrifera*) forests and intertidal green algae (*Ulvophyceae*) with Sentinel-2 imagery," *Remote Sens.*, vol. 12, no. 4, 2020, Art. no. 694.
- [57] A. J. Smola and B. Schölkopf, "A tutorial on support vector regression," *Statist. Comput.*, vol. 14, no. 3, pp. 199–222, 2004.
- [58] S. R. Sain, *The Nature of Statistical Learning Theory*. New York, NY, USA: Taylor & Francis, 1996.
- [59] J. Verrelst et al., "Machine learning regression algorithms for biophysical parameter retrieval: Opportunities for Sentinel-2 and -3," *Remote Sens. Environ.*, vol. 118, pp. 127–139, 2012.
- [60] Y. B. Dibike, S. Velickov, D. Solomatine, and M. B. Abbott, "Model induction with support vector machines: Introduction and applications," *J. Comput. Civil Eng.*, vol. 15, no. 3, pp. 208–216, 2001.
- [61] H. Cao and L. Han, "Drift path of green tide and the impact of typhoon 'Chan-hom' in the Chinese Yellow Sea based on GOCI images in 2015," *Ecol. Inform.*, vol. 60, 2020, Art. no. 101156.
- [62] B. Arabi, M. S. Salama, J. Pitarch, and W. Verhoef, "Integration of in-situ and multi-sensor satellite observations for long-term water quality monitoring in coastal areas," *Remote Sens. Environ.*, vol. 239, 2020, Art. no. 111632.
- [63] E. Sherman, J. K. Moore, F. Primeau, and D. Tanouye, "Temperature influence on phytoplankton community growth rates," *Glob. Biogeochem. Cycles*, vol. 30, no. 4, pp. 550–559, 2016.
- [64] G. Zhang, M. Wu, M. Zhou, and L. Zhao, "The seasonal dissipation of *Ulva prolifera* and its effects on environmental factors: Based on remote sensing images and field monitoring data," *Geocarto Int.*, vol. 37, no. 3, pp. 860–878, 2022.
- [65] S. Wang et al., "Variations of dominant free-floating *Ulva* species in the source area for the world's largest macroalgal blooms, China: Differences of ecological tolerance," *Harmful Algae*, vol. 74, pp. 58–66, 2018.
- [66] H. Li, Y. Zhang, H. Tang, X. Shi, R. B. Rivkin, and L. Legendre, "Spatiotemporal variations of inorganic nutrients along the Jiangsu coast, China, and the occurrence of macroalgal blooms (green tides) in the southern Yellow Sea," *Harmful Algae*, vol. 63, pp. 164–172, 2017.
- [67] X. Zhang, Q. Luan, J. Sun, and J. Wang, "Influence of *Enteromorpha prolifera* (Chlorophyta) on the phytoplankton community structure," *Mar. Sci.*, vol. 37, no. 3, pp. 24–31, 2013.
- [68] C. J. Gobler and W. G. Sunda, "Ecosystem disruptive algal blooms of the brown tide species, *Aureococcus anophagefferens* and *Aureoumbra lagunensis*," *Harmful Algae*, vol. 14, pp. 36–45, 2012.
- [69] H. Gao, R. Su, F. Zhou, C. Zhang, and X. Shi, "Extraction and identification of toxic organic substances from decaying green alga *Ulva prolifera*," *Harmful Algae*, vol. 93, 2020, Art. no. 101786.
- [70] H. Zhang et al., "Role of nutrients in the development of floating green tides in the Southern Yellow Sea, China, in 2017," *Mar. Pollut. Bull.*, vol. 156, 2020, Art. no. 111197.
- [71] D. Fu, Y. Ding, D. Liu, and D. Pan, "Delayed effect of typhoon on marine chlorophyll-a concentration," *J. Trop. Oceanogr.*, vol. 28, no. 2, pp. 15–21, 2009.

- [72] D. Fu, D. Pan, Y. Ding, and J. Zou, "Quantitative study of effects of the sea chlorophyll-a concentration by typhoon based on remote-sensing," *Acta Oceanologica Sin.*, vol. 31, no. 3, pp. 46–56, 2009.
- [73] X. Sun, F. Shen, R. J. Brewin, D. Liu, and R. Tang, "Twenty-year variations in satellite-derived chlorophyll-a and phytoplankton size in the Bohai Sea and Yellow Sea," *J. Geophys. Res., Oceans*, vol. 124, no. 12, pp. 8887–8912, 2019.
- [74] H. Yamaguchi et al., "Seasonal and summer interannual variations of SeaWiFS chlorophyll a in the Yellow Sea and East China Sea," *Prog. Oceanogr.*, vol. 105, pp. 22–29, 2012.
- [75] X. Liu et al., "Seasonal phytoplankton response to physical processes in the southern Yellow Sea," *J. Sea Res.*, vol. 95, pp. 45–55, Jan. 2015.
- [76] F. Zhai, Z. Liu, Y. Gu, S. He, Q. Hao, and P. Li, "Satellite-observed interannual variations in sea surface chlorophyll-a concentration in the Yellow Sea over the past two decades," *J. Geophys. Res., Oceans*, vol. 128, 2023, Art. no. e2022JC019528.
- [77] G. Zhang et al., "Influence of Sea surface temperature on outbreak of *Ulva prolifera* in the Southern Yellow Sea, China," *Chin. Geographical Sci.*, vol. 30, no. 4, pp. 631–642, 2020.
- [78] B. Xiu, S.-K. Liang, X.-L. He, X.-K. Wang, Z.-G. Cui, and Z.-J. Jiang, "Bioavailability of dissolved organic nitrogen and its uptake by *Ulva prolifera*: Implications in the outbreak of a green bloom off the coast of Qingdao, China," *Mar. Pollut. Bull.*, vol. 140, pp. 563–572, 2019.
- [79] J. H. Zhang et al., "Variations of morphology and photosynthetic performances of *Ulva prolifera* during the whole green tide blooming process in the Yellow Sea," *Mar. Environ. Res.*, vol. 92, pp. 35–42, 2013.
- [80] L. Qi et al., "Climate and anthropogenic controls of seaweed expansions in the East China Sea and Yellow Sea," *Geophys. Res. Lett.*, vol. 49, no. 19, 2022, Art. no. e2022GL098185.
- [81] F. Qiao, G. Wang, X. Lü, and D. Dai, "Drift characteristics of green macroalgae in the Yellow Sea in 2008 and 2010," *Chin. Sci. Bull.*, vol. 56, no. 21, pp. 2236–2242, 2011.
- [82] L. Hu, K. Zeng, C. Hu, and M.-X. He, "On the remote estimation of *Ulva prolifera* areal coverage and biomass," *Remote Sens. Environ.*, vol. 223, pp. 194–207, 2019.
- [83] J. Xiao, Z. Wang, D. Liu, M. Fu, C. Yuan, and T. Yan, "Harmful macroalgal blooms (HMBs) in China's coastal water: Green and golden tides," *Harmful Algae*, vol. 107, 2021, Art. no. 102061.
- [84] S. Son, T. Platt, H. Bouman, D. Lee, and S. Sathyendranath, "Satellite observation of chlorophyll and nutrients increase induced by Typhoon Megi in the Japan/East Sea," *Geophys. Res. Lett.*, vol. 33, no. 5, 2006, Art. no. L05607.



Guangzong Zhang received the M.S. degree in geography from Ludong University, Yantai, China, in 2020. He is currently working towards the Ph.D. degree in machine from Harbin Institute of Technology, Shenzhen, China.

His research interests include deep learning and its applications on ocean color of remote sensing and harmful algae image classification.



Lifeng Niu received the M.S. degree in cartography and geographic information system from Lanzhou Jiaotong University, Lanzhou, China, in 2020. She is currently working toward the Ph.D. degree in machine from Harbin Institute of Technology, Shenzhen, China.

Her research interests include machine learning and its applications in nearshore ecological environment.



Mengquan Wu (Member, IEEE) received the M.S. degree in cartography and geographic information system from Wuhan University, Wuhan, China, in 2004, and the Ph.D. degree in geography and geographic information system from the Institute of Remote Sensing Applications, Chinese Academy of Sciences, Beijing, China, in 2007.

Since 2007, he has been a Professor with the School of Resources and Environmental Engineering, Ludong University, Yantai, China. His research interests include remote sensing of marine environment, smart cities, and remote sensing of coastal zones.



Hermann Kaufmann received the M.S. degree in geology and Ph.D. degree in remote sensing from the University of Munich, Germany, in 1980 and 1985, respectively.

From 1993 to 2014, he was with the Remote Sensing Section, German Research Centre for Geosciences, Potsdam, Germany. Since 2014, he has been with the Institute of Space Science, Shandong University at Weihai, Weihai, China. His current research focuses on the hyperspectral remote sensing.



Hanyu Li received the M.S. degree in aerospace science and technology from Harbin Institute of Technology, Shenzhen, China, in 2023. She is currently working toward the Ph.D. degree in environmental planning from Technical University of Berlin, Berlin, Germany.

Her research interests include machine learning and its applications in estimation of nearshore ecological environment.



Yufang He received the M.S. degree in geodesy and survey engineering from Chang'an University, Xi'an, China, in 2019. She is currently working toward the Ph.D. degree in aerospace science and technology from Harbin Institute of Technology, Shenzhen, China.

Her research interests include machine learning and its applications in monitoring of surface subsidence.



Bo Chen (Member, IEEE) received the B.E. degree in aerial photogrammetry and Ph.D. degree in photogrammetric engineering and remote sensing from Information Engineering University, Zhengzhou, China, in 2002 and 2008, respectively.

Since 2020, he has been a Full Professor with the Institute of Space Science and Applied Technology, Harbin Institute of Technology (Shenzhen), Shenzhen, China. His research interests include satellite-on-orbit computing, geospatial Big Data, and spatial information engineering.